

On isolated roughness elements embedded into the laminar boundary layer

Dominik K. Puckert^{1*}, Ulrich Rist¹

¹ Universität Stuttgart, Institut für Aerodynamik und Gasdynamik, Stuttgart, Germany

* puckert@iag.uni-stuttgart.de

Abstract

In this experimental work, the influence of differently shaped roughness elements on a flat-plate, laminar boundary layer is investigated. The roughness elements under consideration are of blunt, cylindrical and streamlined shape. The primary goal is to control the region of local absolute instability and hairpin vortex shedding in the aft recirculation zone. With the blunt roughness, hairpin vortices are observed without subsequent transition in a narrow range of Reynolds numbers. For the cylindrical shape, hairpin vortices evolve into early turbulence. When a streamlined fairing is added to the cylinder to minimize the size of the aft recirculation zone, secondary instabilities grow in the shear of the streaks in the far wake. This leads to transition without the formation of hairpin vortices. The well-known hairpin vortices downstream of roughness elements are therefore not necessarily decisive in the transition process of roughness-disturbed boundary layers.

1 Introduction and set-up

Investigations on three-dimensional (3-D), isolated roughness elements embedded into a laminar boundary layer have received great attention in the last years. Particularly due to their ability to attenuate Tollmien-Schlichting (TS) waves as a means of passive flow control (Fransson et al., 2005), it is important to understand and predict factors leading to early transition through vortex shedding. In most of the literature, the Reynolds number

$$Re_{kk} = \frac{ku_k}{\nu}, \quad (1)$$

based on the roughness height k , kinematic viscosity ν and velocity u_k in the undisturbed boundary layer is changed while the shape remains constant. In contrast, the present investigation aims at a variation of the shape. Such investigations are rather rare and occur mostly in the form of a collection of data from different works such as for instance Gregory and Walker (1956) and Ergin and White (2006). In case of cylindrical roughness elements, the aspect ratio D/k with diameter D has recently been identified as a key factor in the competition between convective and global instabilities (Loiseau et al., 2014; Puckert and Rist, 2018b). Loiseau et al. (2014) conducted a 3-D global stability analysis and found that the leading global mode changes from sinuous to varicose symmetry when the aspect ratio is increased. Sinuous modes can develop into von-Kármán-type of vortex streets, whereas varicose modes tend to develop into hairpin vortices in the non-linear stages. This has been confirmed experimentally by Puckert and Rist (2018a). Hairpin vortices are typically observed behind roughness elements at sufficiently large Reynolds numbers (Acarlar and Smith, 1987). In this context, the critical roughness Reynolds number separates between convective and global instabilities and may easily be confused with transition because of strong amplification of background noise, leading to rapid turbulence (Puckert and Rist, 2018a). For this reason, vortex shedding close to the roughness is of particular interest in this study. Hairpin vortices originate primarily from the recirculation zone (Klebanoff et al., 1992) and it is therefore interesting to control this sensitive region by the shape of the roughness.

The laminar water channel (Laminarwasserkanal, LaWaKa) is a closed-circuit water channel at the Institute of Aerodynamics and Gas Dynamics (IAG) at the University of Stuttgart. The turbulence intensity is 0.05 % of the freestream velocity in the frequency range 0.1-10 Hz at 0.145 ms^{-1} Wiegand (1996). The

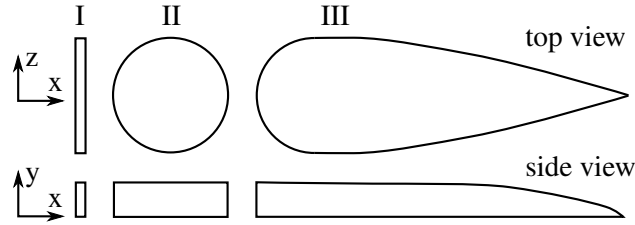


Figure 1: Roughness: blunt rectangle (shape I), cylinder (shape II) and cylinder with fairing (shape III).

test section is $8 \times 1.2 \times 0.2 \text{ m}^3$ large. A two-dimensional, laminar boundary layer of Blasius type is created by a flat plate with elliptical leading edge. Careful suction on the side edges of the flat plate prevents the growth of corner-flow boundary layers. Three roughness elements with identical height k and spanwise extent D but with different shapes are investigated. The three roughness elements under consideration are a blunt rectangle (shape I), a cylinder (shape II) and a cylinder with fairing (shape III) as illustrated in figure 1. The "frontal area" $A_{front} = kD$ of these roughness elements remains the same throughout this work. The roughness elements are placed in the spanwise center of the flat plate at 57.1 from the leading edge. Length scales in this work are non-dimensionalized by $k = 10 \text{ mm}$ and originate at the bottom center of the roughness with x -, y - and z -coordinates extending in streamwise, wall-normal and spanwise directions, respectively. Hot-film anemometry and particle image velocimetry (PIV) are used to acquire data. Details on the data acquisition methods are described in Puckert and Rist (2018a).

2 Transition Reynolds number

The intermittency function γ has been computed to detect turbulence as a function of the Reynolds number Re_{kk} . First, the streamwise velocity u' from hot-film measurements is multiplied by its derivative du'/dt to enhance the sensitivity to turbulence. Continuous wavelet transforms are used to obtain a smooth derivative. The detector function is then group averaged into a criterion function and compared to a threshold value which originates from a reference case in laminar flow. The reference signal is multiplied by a constant factor in the range 1-10 to allow for manual control of the method. Manual adjustments in this method only become necessary when the set-up changes significantly. It has been found that the results do not change noticeably as long as reasonable inputs are given. The intermittency γ is the percentage of turbulence in the total signal and can be estimated by summing up the parts of the signal where the criterion function is greater than the threshold value. An intermittency of 0% or 100% represents laminar or turbulent flow, respectively.

The data to feed this algorithm have been collected by a hot-film probe at a fixed center position at the roughness height at $x = 1650 \text{ mm}$. Previous dye streakline visualizations help to narrow down the possible range of freestream velocities at which transition occurs. Figure 2 shows the intermittency function plotted over Re_{kk} to determine the transition Reynolds number at $\gamma = 50\%$ for the three types of roughness elements as introduced in section 1. In the LaWaKa, transition can be detected at $Re_{kk} = 230, 405,$ and 680 for shape I, II and III, respectively. The different shapes greatly influence the flow around and downstream of the roughness although the wall-normal and vertical roughness dimensions are identical. The accuracy of the intermittency method at the LaWaKa is estimated to be in the order of $Re_{kk} = \pm 20$.

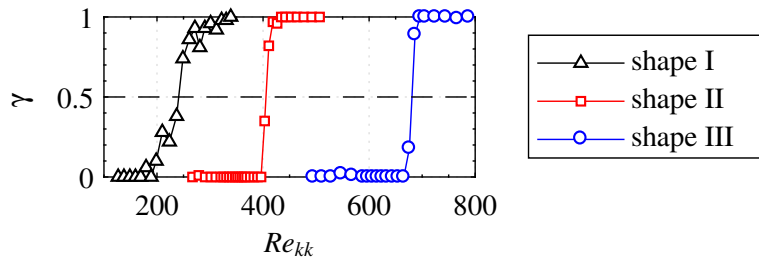


Figure 2: Intermittency estimate as a function of roughness Reynolds number.

3 Instability mechanism

To investigate the frequency spectra, hot-film signals have been recorded at different downstream stations with steps of $\Delta x = 2$ from the trailing edge of the respective shape to $x = 100$. The wall-normal position was $y = 1$ and the measurement time was 30 s at each station. The power spectral density from fast Fourier transforms of the hot-film signals is shown in figure 3 in gray scales for $Re_{kk} = 500$ (shape I and II) and $Re_{kk} = 800$ (shape III). The circular frequency is defined by $\omega = 2\pi f\nu U_e^2$ with the physical frequency f in Hz and the freestream velocity U_e . This circular frequency allows for a comparison to the results of Loiseau et al. (2014). Figure 3(a,b) reveals distinctive frequency bands in the near wake of the roughness with fundamental frequencies of $\omega = 0.7$ ($f = 0.63$ Hz) for shape I and 0.85 ($f = 0.77$ Hz) for shape II, respectively. The lower frequency of shape I may be due to a larger recirculation zone of the blunt roughness shape. For shape III, the flow is still laminar at $Re_{kk} = 500$ and therefore the spectrum for a higher Reynolds number $Re_{kk} = 800$ is illustrated in figure 3(c). Nevertheless, no discrete frequency bands can be observed. It can be inferred from these results that the reduction of recirculation zone in shape III reduces the ability of the flow to resonate or quasi-resonate. Instead, convective instabilities of a broadband frequency range could be the relevant mechanism for this shape. Another possible explanation is that instability occurs first at the outer regions of the roughness wake and not in the spanwise center where the probe was located. This hypothesis needs clarification.

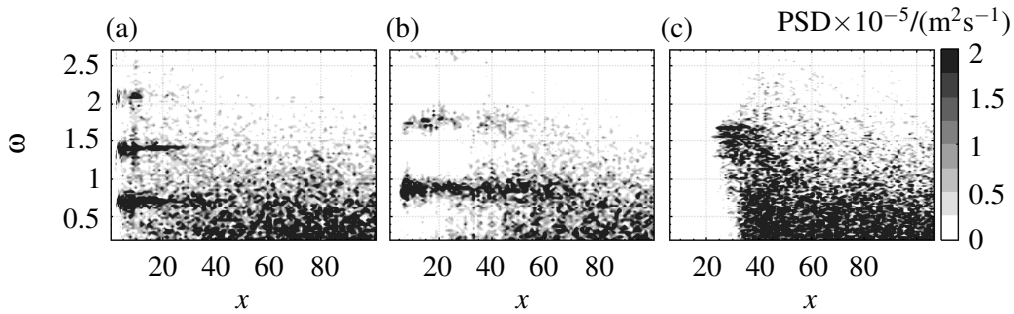


Figure 3: Frequency spectra of (a) shape I at $Re_{kk} = 500$, (b) shape II at $Re_{kk} = 500$ and (c) shape III at $Re_{kk} = 800$.

One of the great benefits of a water channel are visualizations. To resolve the above hypothesis, potassium permanganate crystals are used to draw dye streaklines into the flow. Figure 4 shows pictures of shape I, II and III taken at $Re_{kk} = 200$, 500 and 800, respectively. In figure 4(a), the spatial evolution of hairpin vortices or its remnants can be seen. Interestingly, these vortices decay without triggering transition or turbulence. In contrast, most of the literature relates hairpin vortices to a late stage of transition. As shown here, this is not true in all cases. For shape I, the base flow is strongly disturbed at first, which makes the flow highly unstable in a confined region before it stabilizes again further downstream. This is supported by stability diagrams of Siconolfi et al. (2015) and Dörr and Kloker (2018). These effects are due to strong, localized destabilization by the blunt roughness and have rarely been observed with shape II and never with shape III. The cylindrical roughness (shape II) is portrayed at $Re_{kk} = 500$ in figure 4(b). Upstream and on the sides of the roughness, a horseshoe vortex can be seen. Downstream, hairpin vortices form in the recirculation zone and shed disturbances that are convected downstream. The visualization of shape III is different from the others. Disturbances in figure 4(c) seem to grow from the outside to the inside in the streamwise direction. Furthermore, no hairpin vortices can be observed, which explains the late transition at $Re_{kk,tr} = 680$ for this shape. In contrast to the other shapes, transition in this case may be due to secondary instabilities of the streaks in the roughness wake. Turbulence in this figure is represented by the dark cloud beyond $x = 40$.

To acquire more quantitative data, PIV is used with a Nd:YAG laser pulsed at 10 Hz to illuminate a light-sheet at $y = 1$ downstream of the roughness. For each case, 300 images are recorded at 5 Hz by a PCO SensiCam. The low frequencies of the LaWaKa allow for time-resolved Fourier mode decomposition (FMD). Global power spectra have been computed in the present study as described in detail by Ma et al. (2015). The spectrum for shape I is shown in figure 5(a). Most noticeably, there is a sharp-edged peak at $\omega = 0.94$, which is qualitatively in line with the visual observation of hairpin vortex shedding in figure 4(a). The corresponding real part of the Fourier mode is shown in figure 5(b) as patches of yellow and blue color representing iso-surfaces of 20 % of the maximum disturbances, respectively. Initially, the mode can

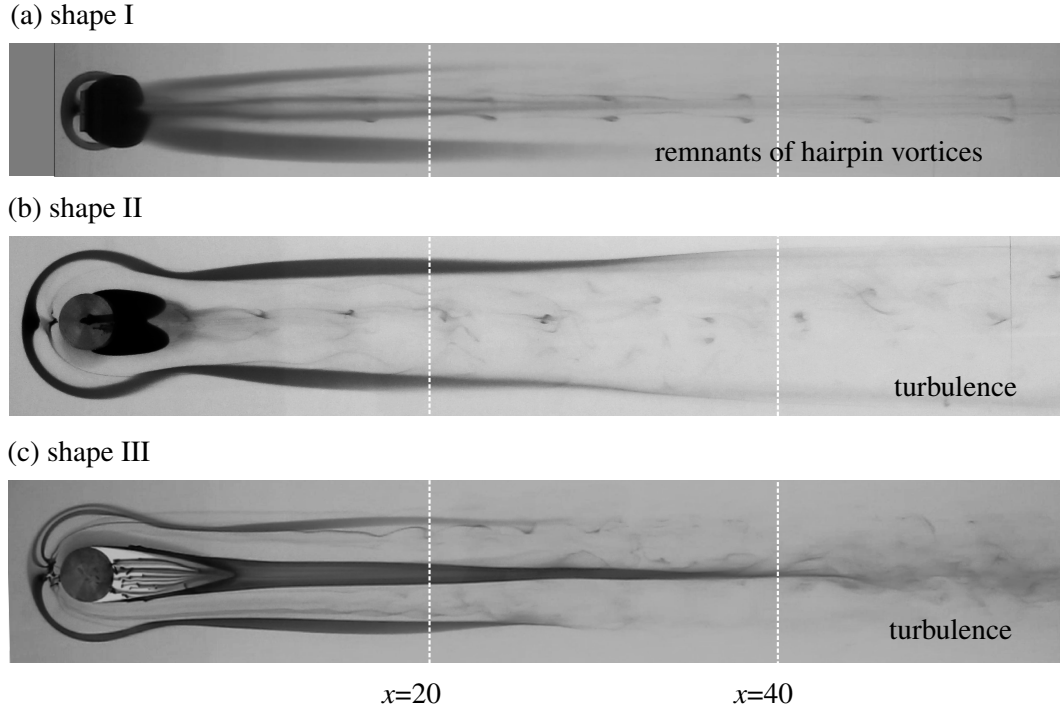


Figure 4: Visualization of (a) shape I at $Re_{kk} = 200$, (b) shape II at $Re_{kk} = 500$ and (c) shape III at $Re_{kk} = 800$.

be described by lambda-shaped legs between $4 < x < 15$, spreading to the sides as the downstream distance increases. As a result, the disturbances become two-dimensional by the end of the domain. However, the flow beyond $x = 17$ may already be part of a late stage of transition, since the Reynolds number of this experiment is beyond the transition Reynolds number (cf. figure 2).

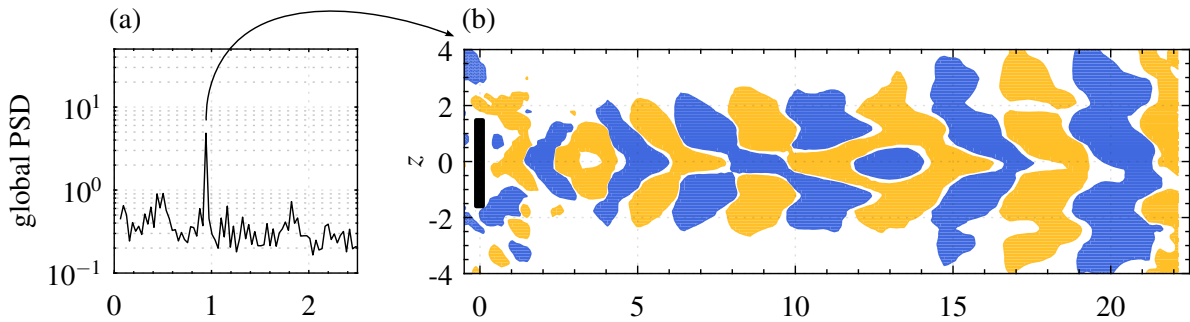


Figure 5: Fourier mode analysis for shape I at $Re_k = 467$, $Re_{kk} = 384$ with (a) global power spectrum and (b) Fourier mode at $\omega = 0.94$. Isosurface of streamwise velocity disturbance, yellow and blue for $\pm 20\%$ of maximum disturbance, respectively.

Figure 6 shows the result from the same method applied to shape II at $Re_{kk} = 429$. This case is slightly beyond the transition Reynolds number as demonstrated in figure 2. The power spectrum in figure 6(a) exhibits a frequency peak at $\omega = 0.807$, which is, however, more broadbanded than in figure 5(a). This is in agreement with the observations of Puckert and Rist (2018b), who found that convective amplification is the dominant mechanism at Reynolds numbers below the critical Reynolds number $Re_{kk,c} = 490$ from predictions by 3-D global linear stability theory (Loiseau et al., 2014). Regarding the real part of the Fourier mode at $\omega = 0.807$ in figure 6(b), this mode exhibits a stripe of disturbances at first and more complex patterns starting at $x = 12$. This confirms that the disturbances evolve from the spanwise center to the outer regions and proves that the first instability in streamwise direction originates from the recirculation zone. The outer disturbances are most likely initiated by hairpin vortices from the recirculation zone and

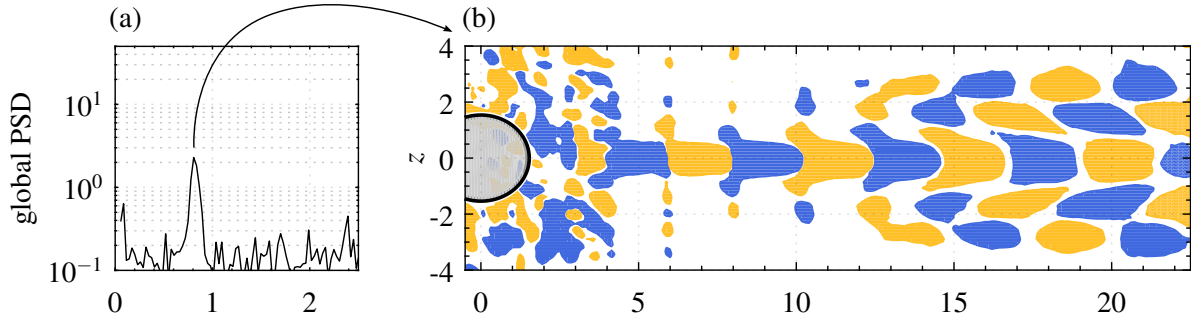


Figure 6: Same caption as figure 5 but with shape II and $Re_k = 509$, $Re_{kk} = 429$, $\omega = 0.807$.

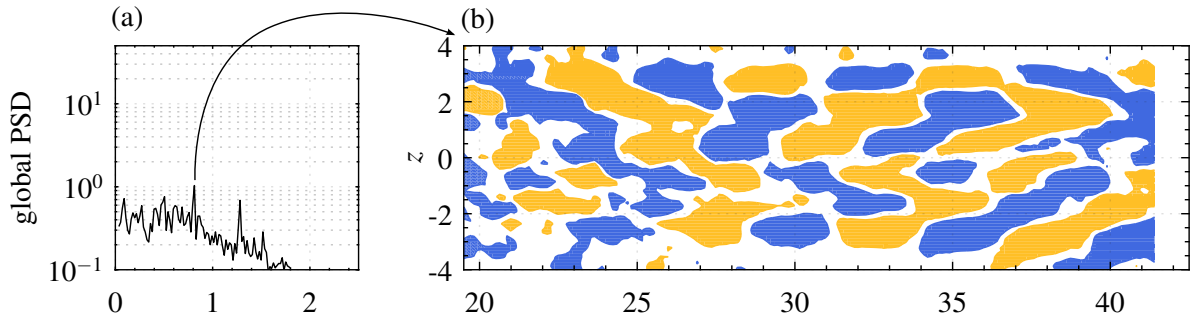


Figure 7: Same caption as figure 5 but with shape III and $Re_k = 813$, $Re_{kk} = 763$, $\omega = 0.812$.

destabilize by the shear of the roughness wake. Overall, the disturbance mode is more pronounced than in figure 5 because of less late-stage transitional effects. Note that the disturbance mode 'spreads' to the sides more closely to the roughness when Re_{kk} is increased (not shown here).

Shape III is – once again – different from the previous cases. The power spectrum in figure 7(a) illustrates two strong frequencies in the spectrum that are not harmonic to each other and can barely be recognized as being peaks in contrast to figures 5(a) and 6(a). Nevertheless, one dominant frequency ($\omega = 0.812$) is fairly close to the peaks in figures 5(a) and 6(a). Therefore, it is reasonable to assume that there is a small remaining tendency of this shape to prefer the frequency at which hairpin vortices would have shed without the streamlined fairing of shape II. An analysis of the real part of the mode $\omega = 0.812$ in figure 7(b) reveals that there are no obvious patterns that could be recognized as a hairpin vortex. Note that this evaluation is performed further aft of the origin of the roughness to account for the more lengthy shape of the streamlined body. An evaluation further upstream does not exhibit any more interesting features and are thus not shown here. The same applies to the second dominant frequency in figure 7(a) at approximately $\omega = 1.3$. Even changing the Reynolds numbers did not reveal any more details except for either laminar or rather unordered portraits. The lack of a clear disturbance mode goes in line with the assumption that streak instabilities from the horseshoe vortex are responsible for the chaotic patches observed in figure 7(b). It can be hypothesized that neither local absolute, nor global, nor primary modal instabilities cause transition behind this streamlined roughness shape. Instead, breakdown to turbulence can rather be understood as a result of secondary instability of the roughness streaks in this case.

4 Discussion

This investigation reveals an ambiguity in the literature. Some authors explain transition behind roughness elements by Kelvin-Helmholtz (KH) instability and subsequent roll-up of hairpin vortices (Klebanoff et al., 1992; Ye et al., 2018) whereas others account bypass transition for this phenomenon (Ergin and White, 2006; Denissen and White, 2008). Klebanoff et al. (1992) provide evidence that the hairpin vortex shedding from blunt roughness elements is due to KH instability. In contrary, transition from shape III in the present investigation was found to be more related to the instability of streaks. Therefore, the shape of the roughness seems crucial for both the transition Reynolds number and the dominant transition mechanism.

Acknowledgements

This work has partially been financed by the Deutsche Forschungsgemeinschaft (DFG) under Reference Number RE 680/32-1.

References

- Acarlar M and Smith C (1987) A study of hairpin vortices in a laminar boundary-layer. Part 1. Hairpin vortices generated by a hemisphere protuberance. *J Fluid Mech* 175:1–41
- Denissen NA and White EB (2008) Roughness-induced bypass transition, revisited. *AIAA J* 46:1874–1877
- Dörr PC and Kloker MJ (2018) Numerical investigations on Tollmien-Schlichting wave attenuation using plasma-actuator vortex generators. *AIAA J*
- Ergin FG and White EB (2006) Unsteady and transitional flows behind roughness elements. *AIAA J* 44:2504–2514
- Fransson JHM, Brandt L, Talamelli A, and Cossu C (2005) Experimental study of the stabilization of Tollmien-Schlichting waves by finite amplitude streaks. *Phys Fluids* 17:054110
- Gregory N and Walker WS (1956) The effect on transition of isolated surface excrescences in the boundary layer. *Aero Res Council R&M* 2779
- Klebanoff PS, Cleveland WG, and Tidstrom KD (1992) On the evolution of a turbulent boundary layer induced by a three-dimensional roughness element. *J Fluid Mech* 237:101–187
- Loiseau JC, Cherubini S, Robinet JC, and Leriche E (2014) Investigation of the roughness-induced transition: global stability analyses and direct numerical simulations. *J Fluid Mech* 760:175–211
- Ma L, Feng LH, Pan C, Gao Q, and Wang J (2015) Fourier mode decomposition of PIV data. *Sci China Tech Sci* 58:1935–1948
- Puckert DK and Rist U (2018a) Experiments on critical Reynolds number and global instability in roughness-induced laminar-turbulent transition. *J Fluid Mech* 844:878–903
- Puckert DK and Rist U (2018b) Global instability in a laminar boundary layer perturbed by an isolated roughness element. *Exp Fluids* 59
- Siconolfi L, Camarri S, and Fransson JHM (2015) Boundary layer stabilization using free-stream vortices. *J Fluid Mech* 764
- Wiegand T (1996) *Experimentelle Untersuchungen zum laminar-turbulenten Transitionsprozess eines Wellenzugs in einer Plattengrenzschicht*. Ph.D. thesis. Universität Stuttgart
- Ye Q, Schrijer FFJ, and Scarano F (2018) On Reynolds number dependence of micro-ramp-induced transition. *J Fluid Mech* 837:597–626